This article was downloaded by:
On: *22 January 2011*
Access details: *Access Details: Free Access*
Publisher *Taylor & Francis*
Informa Ltd Registered in England and Wales Registered Number: 1072954 Registered office: Mortimer House, 37-41 Mortimer Street, London W1T 3JH, UK

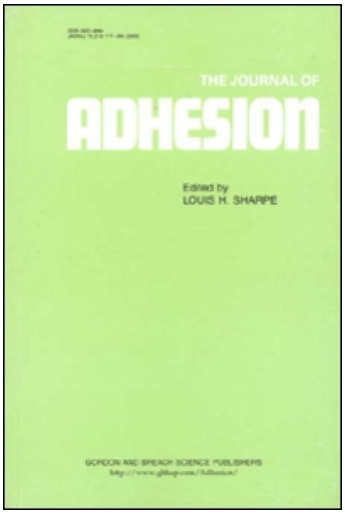

The Journal of Adhesion

Publication details, including instructions for authors and subscription information:
http://www.informaworld.com/smpp/title~content=t713453635

On the Use of Laminated Beams for the Determination of Pure and Mixed-Mode Fracture Properties of Structural Adhesives

K. M. Liechti[a]; T. Freda[a]

[a] Engineering Mechanics Research Laboratory, Department of Aerospace Engineering and Engineering Mechanics, The University of Texas at Austin Austin, TX, U.S.A.

To cite this Article Liechti, K. M. and Freda, T.(1989) 'On the Use of Laminated Beams for the Determination of Pure and Mixed-Mode Fracture Properties of Structural Adhesives', The Journal of Adhesion, 28: 2, 145 — 169

To link to this Article: DOI: 10.1080/00218468908030880

URL: http://dx.doi.org/10.1080/00218468908030880

PLEASE SCROLL DOWN FOR ARTICLE

Full terms and conditions of use: http://www.informaworld.com/terms-and-conditions-of-access.pdf

This article may be used for research, teaching and private study purposes. Any substantial or systematic reproduction, re-distribution, re-selling, loan or sub-licensing, systematic supply or distribution in any form to anyone is expressly forbidden.

The publisher does not give any warranty express or implied or make any representation that the contents will be complete or accurate or up to date. The accuracy of any instructions, formulae and drug doses should be independently verified with primary sources. The publisher shall not be liable for any loss, actions, claims, proceedings, demand or costs or damages whatsoever or howsoever caused arising directly or indirectly in connection with or arising out of the use of this material.

J. Adhesion, 1989, Vol. 28, pp. 145–169
Reprints available directly from the publisher
Photocopying permitted by license only
© 1989 Gordon and Breach Science Publishers, Inc.
Printed in the United Kingdom

On the Use of Laminated Beams for the Determination of Pure and Mixed-Mode Fracture Properties of Structural Adhesives†

K. M. LIECHTI and T. FREDA

Engineering Mechanics Research Laboratory, Department of Aerospace Engineering and Engineering Mechanics, The University of Texas at Austin Austin, TX 78712, U.S.A.

(Received July 7, 1988; in final form November 8, 1988)

Downloaded At: 15:14 22 January 2011

The use of cracked laminated beam specimens is proposed for determining fracture properties of structural adhesives. Slight variations in specimen geometry and loading are used to produce pure mode I and II conditions as well as an intermediate mode-mix. Bounds are established for proper use of the specimens and mixed-mode fracture criteria are examined.

KEY WORDS Structural adhesives; mixed-mode fracture; laminated beam specimens; finite element analysis.

INTRODUCTION

The feasibility of using adhesives to join primary structural parts has been established for some time now. One consideration in designing such adhesively bonded joints is the possibility of crack growth either within the adhesive or at or near the boundary between the adhesive and adherend. The crack growth could be of a catastrophic nature if the fracture toughness of the adhesive or interface has been exceeded or it could be subcritical under fatigue loading, due to viscoelastic effects or under environmental attack. Since crack growth is involved, it is natural to express the resistance to fracture in terms of some fracture parameter that reaches a critical value for catastrophic growth or that can be used for correlations with crack growth rates in the subcritical cases. Because the adhesive layer is usually constrained by stiffer and tougher adherends, the crack growth in structural joints is likely to remain of a mixed-mode nature for initiation and propagation, certainly involving the opening and forward shear

† Presented at the Eleventh Annual Meeting of The Adhesion Society, Inc., Charleston, South Carolina, U.S.A., February 21–24, 1988.

components (mode I and II, respectively) and possibly some antiplane shear (mode III). The question as to the appropriate choice of mixed-mode fracture parameter has received a lot of attention in the area of interlaminar delamination both in composites and adhesives. In reviewing some of the data that has accumulated over the years, the general picture that is emerging[1] is that crack growth in tough materials is governed by the total energy release rate, G_T, whereas in brittle systems the mode II toughness is greater than the mode I toughness, although the fracture envelope is still linear. In view of the fact that different parameters control crack growth, it is probably better—particularly when developing new matrix materials and adhesives—to determine the fracture behavior over the full range of mode-mixes from pure mode I to pure mode II, including some intermediate mode-mixes. The objective of the work presented here was to develop small specimens that could be used to evaluate the pure and mixed-mode fracture resistance of newly-developed adhesives and surface preparations in order to provide direct feedback to formulators in terms of parameters that are used directly in the design process. Another requirement was that the specimens be relatively easy to fabricate, test and extract data from in order to encourage wide use within the adhesives community.

Downloaded At: 15:14 22 January 2011

Ripling and Mostovoy pioneered the use of of fracture mechanics in the evaluation of adhesives and reviewed[2] the performance of the double cantilever beam (DCB) in tapered and untapered form for mode I properties and a prismatic specimen for mode II properties. While the DCB specimens performed well, questions were raised about the prismatic mode II specimen because $G_{IIc} = 20G_{Ic}$ and crack propagation was not in shear but rather by mode I microcracking from the interface of each adherend at 45° to the plane of the bond. Intermediate mode-mixes were later provided by scarf joint specimens[3,4,5] and an independently loaded mixed-mode specimen (ILMMS). In both cases it was found that the orientation of the bond relative to the applied load(s) strongly affected the toughness of the adhesive. Other mode I and mode II specimens that have been considered were compact tension and shear specimens.[6] It was found that the mode I and II toughnesses were approximately the same for primary amine adhesives, but the mode II toughness of a tertiary amine was considerably greater than the mode I value. However, the data (particularly mode II) displayed an unexplained dependence on crack length.

About the same time, the cracked lap shear specimen was introduced[7] as a mixed-mode specimen whose mode-mix could be altered by the relative thickness of the adherends to yield G_I/G_T values generally ranging from 20 to 35%. Although difficulties were noted in using it in the originally proposed form,[8,9] due mainly to interpretation of boundary conditions, it has been extensively used in a simpler way.[10–14] The specimen has been the subject of an ASTM Round Robin Analysis[15] which further emphasized the need for accounting for geometrical nonlinearities[9,16] when analyzing the specimen. Although the cracked lap shear specimen can be tapered to produce $G_I/G_T = 0$[13], the trend in interlaminar delamination studies has been to consider other loadings of symmetric and

unsymmetric laminated beams to obtain pure mode II and more mode I dominant mode-mixes.

The general principle was established in Ref. 17, and more recently in Ref. 18, by considering an asymmetrically loaded double cantilever beam specimen. Pure mode II can be obtained by placing the specimen in three-point bending, in which case it has been dubbed the end-notched flexure (ENF) specimen.[19,20] An alternative is to clamp the laminated beam at one end and subject it to a shear load at the other end.[21] The analysis of the specimen was extended[22–25] to examine the effects of large deflections, transverse shear and friction between the crack faces. The results indicated that while large deflections or transverse shear (depending on specimen design philosophy) might be important, particularly when testing tough materials, frictional effects should be small, as experiments had earlier indicated.[20] The first use of the ENF specimen for measuring adhesive fracture toughness is noted in Ref. 26. A relatively tough adhesive, bonding composite adherends, was tested in mode I, mode II and mixed-mode (G_I/G_T = 23% and 55%) and exhibited essentially equal toughnesses in all cases. The 55% mode-mix ratio was provided by a variation on the mixed-mode flexure (MMF) specimen[20] in which a cracked lap shear specimen was loaded in three-point bending. Again in adhesively-bonded composites, more mode I dominant mode-mixes ($G_I/G_T > 85\%$) have been obtained by using DCB specimens that had adherends of different thickness,[27] although indications were that crack growth was driven to the interface between the thinner adherend and adhesive. While this may be a problem for brittle matrix composites,[27] it might be used to advantage in assessing interfacial durability in metallic joints under environmental attack.

Downloaded At: 15:14 22 January 2011

In view of the desire in the present study to characterize the fracture behavior of adhesives over the full range of mode I to mode II conditions while maintaining simplicity and compactness, consideration has been given to using DCB, ENF and MMF specimens for G_I/G_T ratios of 100%, 0% and 57%, respectively. While DCB specimens having metallic adherends have been extensively used, at the time of program inception, the ENF and MMF specimen had only been used with composite adherends. The high strength of the composites meant that yielding in the adherends was not an issue. However, for the metallic adherends considered here and in some recently published work,[28,29] the adherends must be made thick enough to avoid yielding, thereby simplifying the data reduction. The following sections describe the analysis and testing of the three specimens and present fracture toughness data for FM300 (American Cyanamid), in order to provide guidelines for the use of specimens.

SPECIMEN FABRICATION AND TESTING

The specimens considered in this study were the double cantilever beam (DCB), end-notched flexure (ENF) and mixed-mode flexure (MMF) for pure

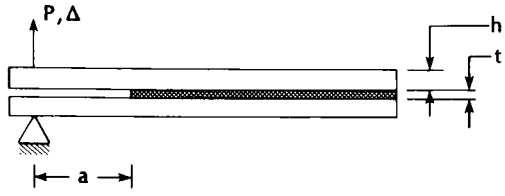

a) Double Cantilever Beam (DCB)

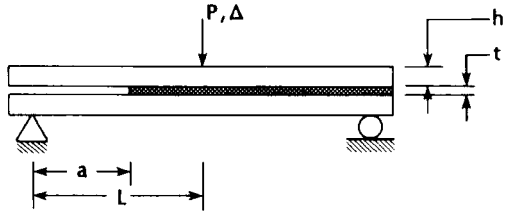

b) End-Notched Flexure (ENF)

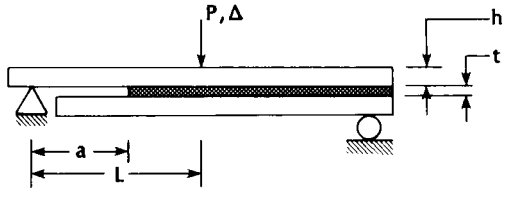

c) Mixed-Mode Flexure (MMF)

L=50.8 mm, h=6.25 mm, t=0.20 mm

FIGURE 1 Laminated beam fracture specimens.

mode I, pure mode II and mixed-mode fracture toughnesses, respectively. Pending the development of a new high-temperature (700°F) adhesive, specimen analysis and development was based on aluminum adherends bonded to FM300† and tested under room temperature conditions. The specimen geometries are shown in Figure 1 and were essentially driven by the constraints of the ENF specimen for which the highest fracture toughnesses were anticipated. A nominal length of 100 mm and a width of 1.27 mm were chosen in order to limit the amount of adhesive per specimen. In view of the lower stiffness and strength of aluminum compared to fiber reinforced composites, the adherend thickness was

† Product of American Cyanamid whose furnishing of material is gratefully acknowledged.

Downloaded At: 15:14 22 January 2011

relatively large at 6.25 mm. The eventual high-temperature application and use of titanium would relax the thickness requirement which ensures that yielding in the adherends does not occur prior to crack growth in the adhesive.

The specimens were sliced from a 20×30 cm bonded panel. The bonded surfaces of the plates making up the panel had been solvent wiped, vapor degreased, scrubbed with cleanser, rinsed with water and etched with a sodium dichromate/sulfuric acid paste. After a distilled water rinse, the panels were oven dried and then primed with BR127.‡ The vacuum-dried adhesive was then applied between the plates which were separated by spacers to ensure a uniform adhesive layer thickness of 0.20 mm. Curing followed standard manufacturers' recommendations.[30] The sliced edges of the specimens were polished to aid in the visual determination of crack length. Each specimen was then given a precrack of approximately 12–20 mm by wedging a razor blade between the adherends so that the crack tip was beyond the edges of the razor. This gave each specimen an initial crack in mode I. In view of the different modes provided by the ENF and MMF specimens, data from this initial crack was always disregarded.

As indicated in Figure 2, the DCB specimen was subjected to a tensile load in the usual manner while the ENF and MMF specimens were subjected to three-point bending. The DCB adherends were connected to the loading device actuators through U-joints and aircraft-type rod ends that transferred the load in a direct manner, free from any measurable moment. The ENF and MMF specimens were supported by roller pins which allowed the support points on the specimen to move freely. Loads were measured by load cells attached to the stationary crosshead of the loading device and the load point displacement by a direct current differential transducer (DCDT). Crack length was measured optically using a microscope and a 0.127 mm resolution scale attached to the specimen. A video camera, monitor and recorder were attached to the microscope so that the crack tip region could be monitored during loading.

Each specimen was loaded at a constant displacement rate until the onset of crack propagation. The displacement was then held constant while the crack arrested and the load dropped. Following arrest, the new crack length was measured and the specimen was partially unloaded before reloading so that compliance measurements could be made. This procedure was subsequently modified in light of plasticity effects associated with the arrested cracks that then became the starter cracks for the next test in a given specimen. In some of the data presented here the arrested cracks were extended in fatigue prior to reloading.

Each load-displacement record (Figure 3) was used to determine specimen compliance as a function of crack length. In the DCB and MMF specimens crack initiation occurred at the maximum load. However, in the ENF specimen, the video recordings revealed that crack initiation occurred prior to the attainment of maximum load and the critical load was therefore associated with deviation from

‡ The adherend surface preparation processes were developed and carried out by personnel of Hughes Aircraft Company. Their assistance in this step is gratefully acknowledged.

Downloaded At: 15:14 22 January 2011

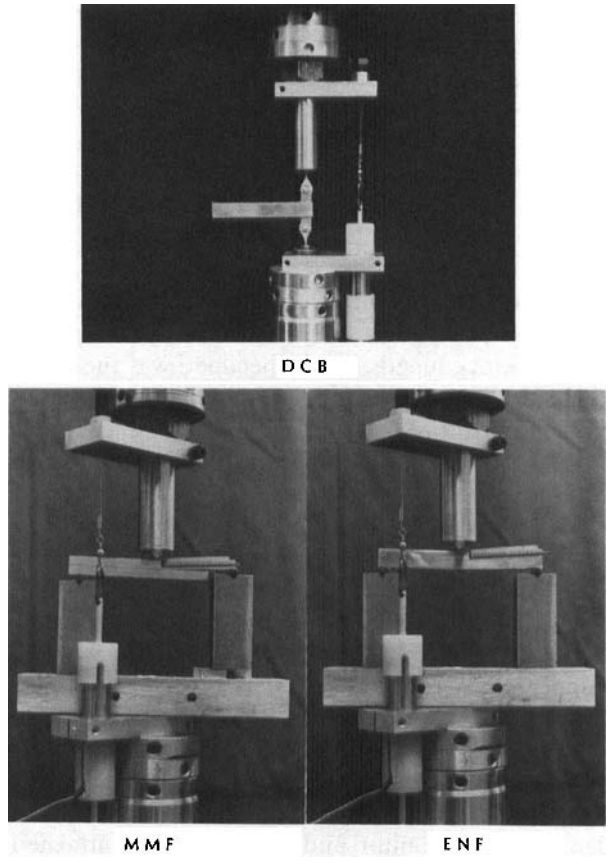

FIGURE 2 Loading rigs for the fracture specimens.

Downloaded At: 15:14 22 January 2011

the linear response. For each load arrangement, the compliance of the machine and fixturing was determined by substituting a much stiffer bar in the place of the specimen and was subsequently subtracted from the measured specimen compliance.

The adhesive stress–strain behavior was determined from a bulk sample of FM300 for later use in linear elastic and elastoplastic stress analyses of the specimens. Four layers of adhesive tape were cured together into one sheet following the same cycle as was used in bonding the joint specimens. Strips measuring $15.24 \times 1.27 \times 0.10$ cm were sliced from the sheet and subjected to uniaxial tension at a constant grip displacement rate of 6.35×10^{-6} m/s. The longitudinal and transverse strains were measured with an averaging biaxial extensometer. The stress strain behavior is shown in Figure 4, for a Young's modulus of 2.28 GPa, Poisson's Ratio of 0.4 and a yield strength of 20 MPa. The piecewise linear and elastic perfectly plastic representations that were used in the stress analyses are also shown in Figure 4.

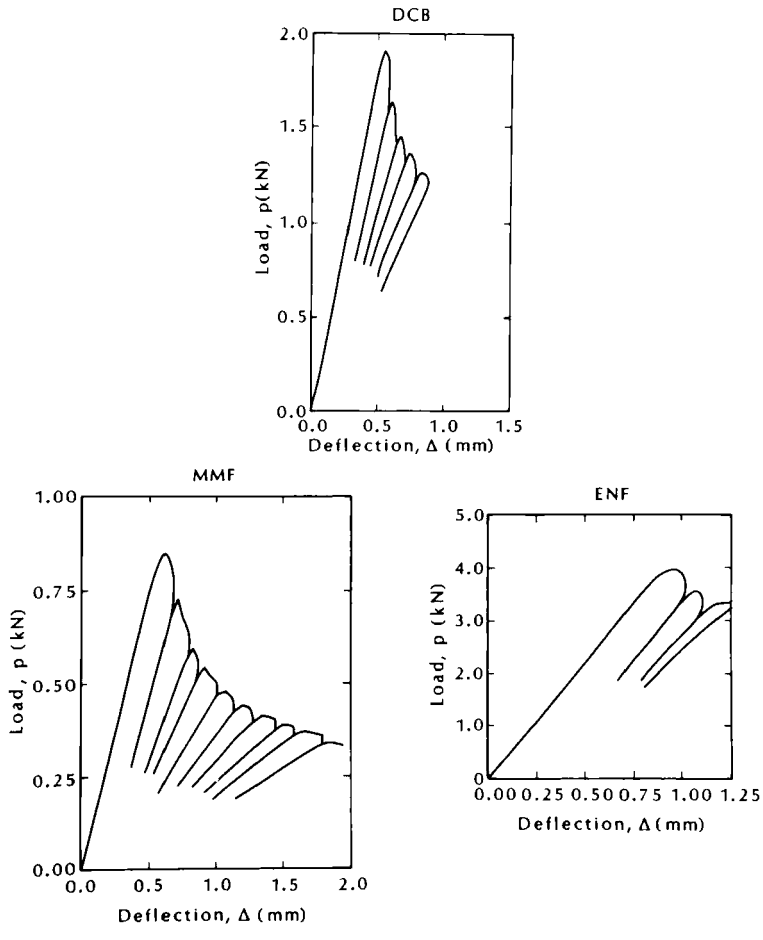

FIGURE 3 Load deflection response of the fracture specimens.

ANALYSIS

The critical values of strain energy release rates were determined from the measured compliance, beam theory and finite element analysis. For the measured compliance and beam theory, the total strain energy release rate, G_T, for a given load, P, was obtained from the rate of change of compliance, C, with crack length, a, through

$$G_T = \frac{P^2}{2b}\frac{\partial C}{\partial a} \tag{1}$$

where b is the specimen width. The compliance was also used as the basis for determining the validity of the beam theory and finite element analyses.

Downloaded At: 15:14 22 January 2011

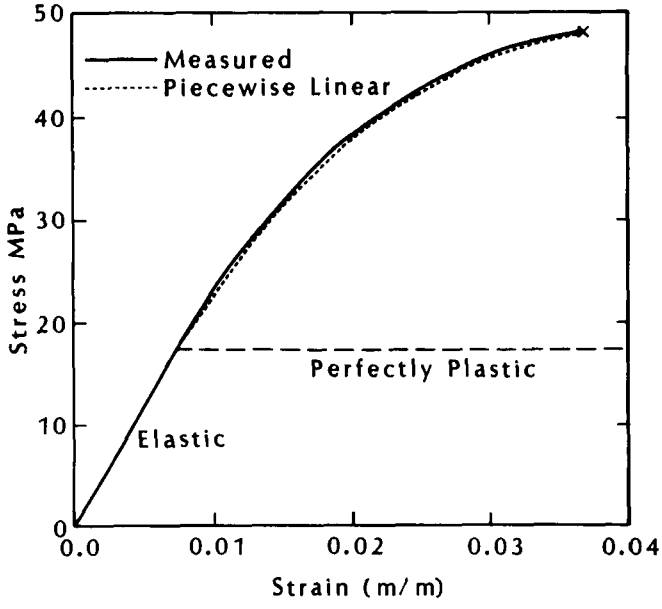

FIGURE 4 Uniaxial tension deformation of neat adhesive film.

Downloaded At: 15:14 22 January 2011

The beam theory analyses for the deflections of the three specimens included the component due to shear in addition to the usual bending deflections because of the relative shortness of the specimens. The compact nature of the specimens and the deflections from Figure 3 confirm that large deflections or geometrical nonlinearities did not have to be accounted for. The compliance of the specimens was taken to be the ratio of the load point deflection, Δ, to the applied load, P, and the expression for each specimen is given below in Eqs. (2), (3) and (4) for the DCB, MMF and ENF specimens, respectively.

$$C_I = \frac{8a^3}{Ebh^3} + \frac{3a}{Gbh} \tag{2}$$

$$C_{I,II} = \frac{2L^3 + 7a^3}{8Ebh^3} + \frac{0.6L + 0.45a}{Gbh} \tag{3}$$

$$C_{II} = \frac{2L^3 + 3a^2}{8Ebh^3} + \frac{1.2L + 0.9a}{4Gbh} \tag{4}$$

where E and G are the tensile and shear moduli, respectively, of the adherends. Details of the analysis are given in Ref. 3.

The mode-mix in each specimen was determined by finite element analysis, although a method for partitioning modes from local values of bending moments and loads without the need for finite element analysis has recently been proposed.[18] The finite element analysis was also used to examine crack face contact and plasticity effects in the ENF specimen. The analyses were conducted

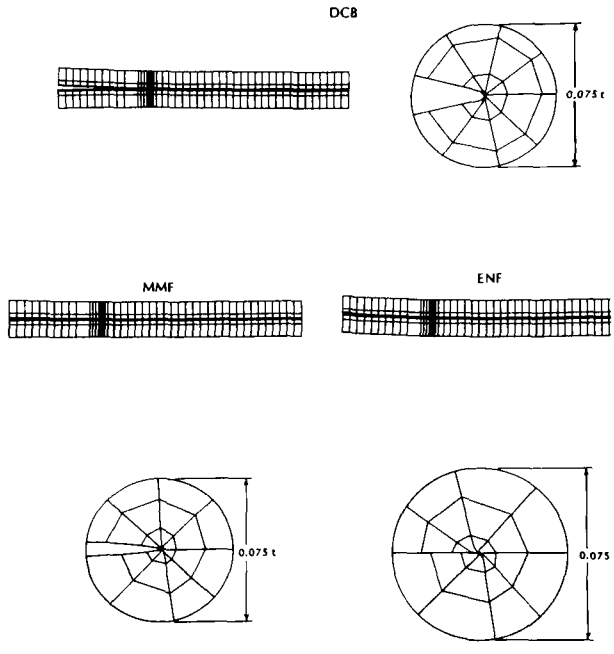

FIGURE 5 Meshes for the finite element stress analysis of the fracture specimens.

using the finite element code ABAQUS.† The adhesive layer was included in the analysis and cracks were taken to be cohesive, coplanar with the middle plane of the adhesive thickness. In view of later comments describing the actual crack growth mechanisms, the assumption of coplanar growth, particularly under mode II conditions may be severe. However, the assumption is a common one and the analysis of tortuous cracks, though interesting, was beyond the scope of the present study.

As the deformed meshes (Figure 5) show, eight node isoparametric quadrilateral elements were used away from the crack tip, which was itself modelled by triangular collapsed quadrilaterals with quarter point nodes. Initially, the constitutive behavior of the adherends and adhesive was taken to be linearly elastic and the boundary conditions were those implied by Figure 1. In the ENF specimen this meant that the cracked end of each adherend was restricted from vertical motion, the same condition that was applied in the beam theory analysis. Although the ABAQUS code calculates the J-integral from contours near the crack tip, the strain energy release rate was actually determined from crack opening displacements due to some discrepancies that were noted in the J-integral

† We are grateful to Hibbitt, Karlsson & Sorenson, Inc., for making ABAQUS available under an academic license.

Downloaded At: 15:14 22 January 2011

results. For an edge-cracked homogeneous plate, the two calculations compared favorably with the theoretical result. However, for the thin bondlines encountered here, the J-integral result was almost exactly one half of the value obtained from the crack opening displacements, which itself was in good agreement with the values from the measured and beam theory compliances.

The analysis just described was later extended in the case of ENF specimen to include the possibility of crack face contact and plastic behavior of the adhesive layer. When each adherend of the crack portion of the specimen was restrained from vertical motion at its end, each adherend deflected in the same way and there was no crack face contact. However, this boundary condition did not fully represent the test condition in which the end reaction was transferred from the lower adherend to the upper adherend by crack face contact. In order to assess this condition more fully, interface elements were placed between the crack faces to prevent their interpenetration when the previous restraint on the vertical end deflection of the upper adherend was relaxed. The effect of friction was also explored by assigning coefficients of friction ranging from 0.2 to 3.0 to the interface elements.

The elastoplastic analysis was carried out for a crack length of 3.18 cm and a load of 3.2 kN, corresponding to crack initiation in one of the tests. The piecewise linear approximation to the stress strain behavior (Figure 4) was employed for the adhesive in the region four elements removed from the crack tip. In order to obtain convergence, it was necessary to assume elastic-perfectly plastic behavior (Figure 4) closer to the crack tip. Yielding was assumed to be governed by the Von Mises criterion.

Downloaded At: 15:14 22 January 2011

RESULTS

The edges of the specimens had been polished prior to testing and that, combined with the blue color of the adhesive, made observation of the crack tip region possible without the need for any other crack tip location enhancing procedures. The scrim cloth fibers could be seen very clearly and played an important role in that way that the main crack propagated. The scrim fibers were grouped in pairs which appeared to be in contact (Figure 6a). The contacting fiber pairs were themselves grouped in pairs about 0.25 mm apart. The distance between each group of pairs was approximately 0.50 mm. In all three types of specimen the extension of the main crack was preceded by whitening of the adhesive around one or two fiber pairs ahead of the main crack. The whitening was then followed by the initiation and growth of microcracks, whose orientation with respect to the bond plane depended on the type of specimen (Figure 6b). For the DCB specimen the microcracks were generally parallel to the bond plane, with slight variations due to the variation in the location of the fiber pairs through the thickness of the adhesive. Growth of the main crack occurred by linking with the microcrack closest to the main tip. In the MMF specimen the microcracks were oriented 25–30° to the bond plane (Figure 6b) and linked up before growing all

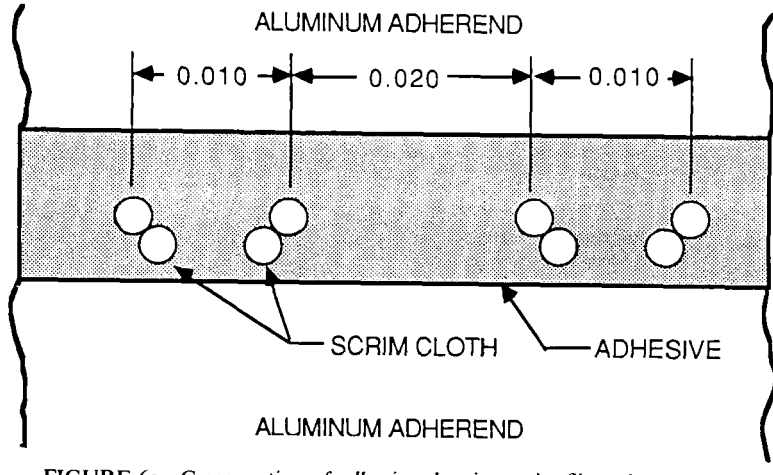

FIGURE 6a Cross-section of adhesive showing scrim fiber placement.

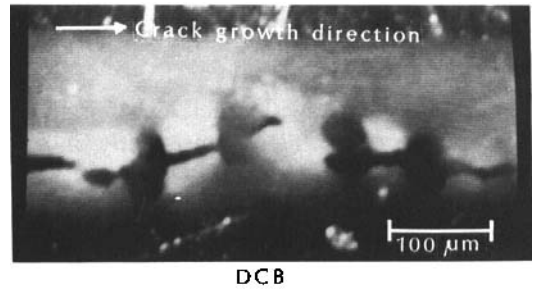

DCB

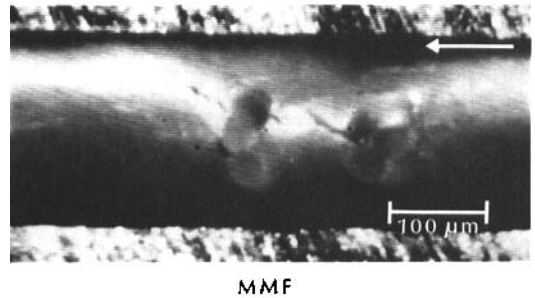

MMF

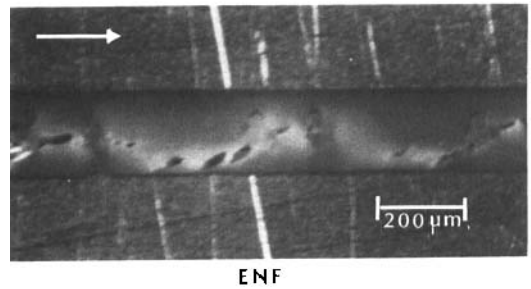

ENF

FIGURE 6b Crack growth mechanisms.

Downloaded At: 15:14 22 January 2011

the way to the interfaces between the adhesive and the adherends. Thus, the fracture surfaces were rougher than those of the double cantilever specimen. The orientation of the microcracks with respect to the bond plane of the ENF specimens was even greater, running from 40–45°. Again the crack growth was cohesive but gave rise to much rougher fracture surfaces than has been observed in the DCB and MMF tests. The scrim cloth fibers therefore acted as stress concentrators causing microcracks to grow from both sides of a contacting fiber pair, their orientation seemingly governed by that of the maximum principal stress. The varying tortuosity of the crack path from one type of specimen to another should be borne in mind as the results, based on the assumption of coplanar growth, are presented. The results are presented by specimen type and consist of comparisons of compliances, determination of mode-mix ratios and corresponding fracture toughnesses. A distinction is made between starter cracks that were simply the arrested crack of the previous test and those that were formed by fatigue crack growth between tests.

Downloaded At: 15:14 22 January 2011

Double cantilever beam

The variation of the DCB compliance with crack length is shown in Figure 7. The compliance from the beam theory Eq. (2) is consistently lower than the measured values and those predicted by the finite element analysis. This is to be expected since, in the beam theory analysis, the cracked beam halves were assumed to be cantilevered at the crack tip, whereas rotation of the adherends actually takes

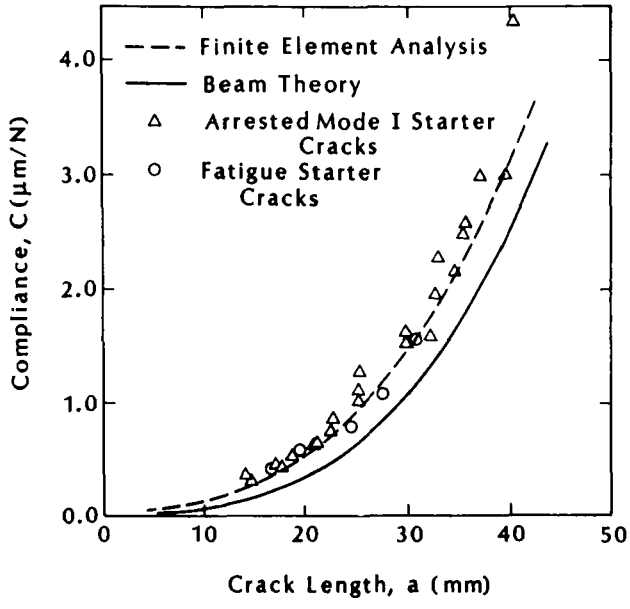

FIGURE 7 Comparison of measured and predicted DCB compliance.

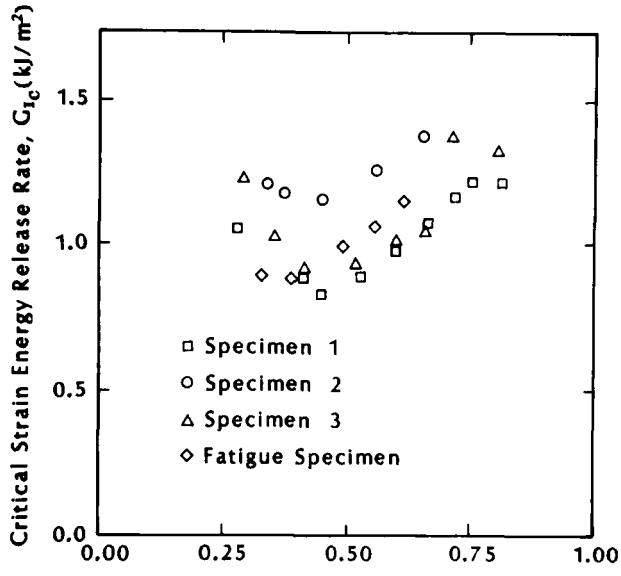

FIGURE 8 Mode I fracture toughness of FM300.

Downloaded At: 15:14 22 January 2011

place beyond the crack tip. The finite element predictions of compliance were slightly less than the measured values, with the difference increasing with crack length. The type of starter crack did not appear to have much effect on the measured compliance. The finite element analysis confirmed, and the deformed mesh (Figure 5) illustrates, that the energy release rates derived from Eqs. (1) and (2) were pure mode I.

The measured compliances were fit to third-degree polynomials[30] so that fracture toughnesses could be determined by direct differentiation. The resulting mode I toughnesses are shown in Figure 8. All the arrested starter cracks gave rise to G_{I_C} values that first decreased and then increased with crack length. The data obtained from fatigue starter cracks only exhibited the increase associated with longer cracks. The initial decrease in G_{I_C} may be associated with the proximity of the applied load or incorrectly applied boundary conditions. The subsequent increase could not have been due to end effects because the longest crack was 50% of the specimen length. The fracture toughnesses were also derived from the beam theory and finite element analyses. The values from beam theory were calculated *via* the compliance relations (1) and (2), while the linear elastic finite element results were scaled to the critical load through

$$G_{I_C} = G_{I_F}\left(\frac{P_C}{P_F}\right)^2 \tag{5}$$

where G_{I_F} was the strain energy release rate associated with the load P_F used in the finite element analysis. The mean values of fracture toughness derived from each method are listed in Table I along with the coefficients of variation. The

TABLE I
Summary of averaged toughnesses

Method of data reduction	Mean G_{I_C} (kJ/m^2)	CV (%)	Mean G_{I,II_C} (kJ/m^2)	CV (%)	Mean G_{II_C} (kJ/m^2)	CV (%)
Measured compliance	1.120	14	1.103	16	1.593	42
Measured compliance†	1.015	25	0.963	11	1.785	45
Beam theory	0.822	17	1.208	35	1.978	66
Beam theory†	0.858	12	1.120	31	2.048	28
Finite element	0.980	16	1.295	14	2.258	57
Finite element†	0.910	17	1.190	12	2.223	21

† Indicates pre-cracks grown by fatigue.

values obtained from the measured compliance were the highest, due to the fact that their slopes were highest (Figure 7). The fatigue precracking did not lead to significantly lower toughness values, which indicates that the arrested starter cracks were sufficiently sharp. For later comparison, G_{I_C} was taken to be 1.12 kJ/m^2, the value from the measured compliances of the arrested cracks. The standard deviations are quite reasonable, except for the measured compliance result for fatigue starter cracks. The rather high value reflects the small number of tests that were conducted.

Downloaded At: 15:14 22 January 2011

Mixed mode flexure

The variation in the compliance of MMF specimens with crack length is shown in Figure 9. For crack lengths greater than 2.5 cm, the compliance derived from finite element analysis was increasingly greater than that obtained from beam theory. Although the difference is not large, the result is surprising because the beam theory analysis should be more applicable at longer crack lengths. Both sets of measured compliances were consistently higher than the predictions. The effect of fatigue precracking was small but did result in slightly lower compliances. The finite element analyses indicated that the mode I energy release rate was 57% of the total value and the mode-mix was independent of crack length.[30] The mixed-mode fracture toughnesses derived from the measured compliances are summarized in Figure 10. For each specimen, the values were reasonably independent of crack length for $a/L < 0.75$. The strong increase thereafter would seem to indicate some interaction between crack tip fields and those due to the central load point. Mean values of mixed-mode fracture toughnesses derived from the three methods are compared in Table I. Fatigue precracking gave rise to G_{I,II_C} values that were about 8% lower than those that were obtained from arrested starter cracks—about the same as was observed in the DCB results. The consistency of the data is good, except for the beam theory results, and could have been further improved by neglecting values for $a/L > 0.74$. The G_{I,II_C} value of 1.10 kJ/m^2 from the arrested starter cracks was much the same as the mode I value.

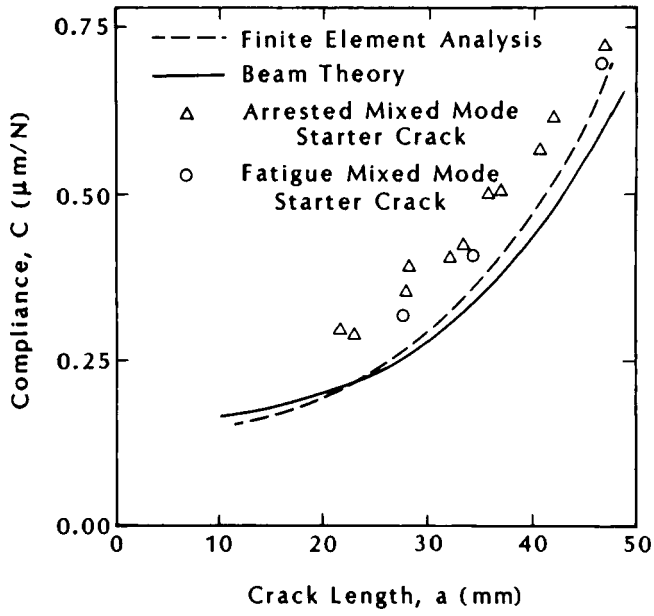

FIGURE 9 Comparison of measured and predicted MMF compliance.

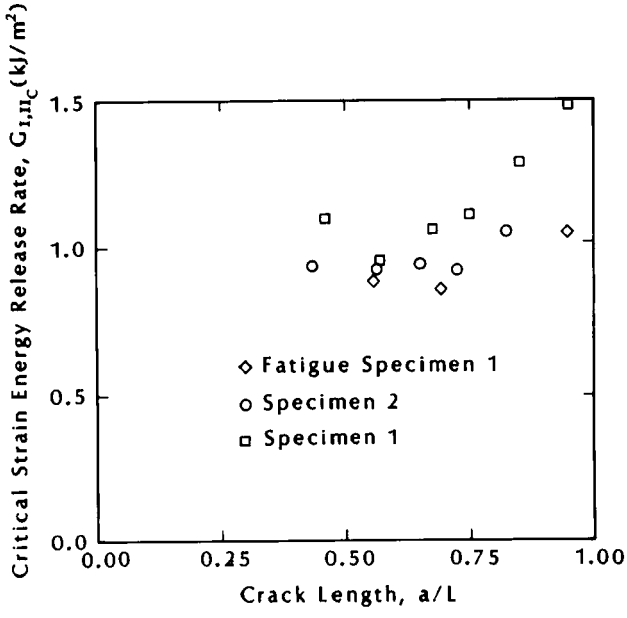

FIGURE 10 Mixed-mode fracture toughness of FM300.

Downloaded At: 15:14 22 January 2011

Downloaded At: 15:14 22 January 2011

End-notched flexure

Five sets of data are recorded in the ENF compliances of Figure 11. The boundary conditions that gave rise to the finite element results shown here were the same as those that were employed in the beam theory analysis. The agreement in compliance is good and was essentially unchanged (<2%) when crack face contact and frictional effects were considered in the finite element analysis, thus confirming similar results from mode II interlaminar delamination.[23,25] Also shown in Figure 11 are the measured compliances of cracks grown in mode I and mode II, with a distinction being made between arrested and fatigue mode II starter cracks. The mode I data were obtained by wedging a specimen to produce a given crack length and then loading in three-point bending to a load level that was insufficient for crack initiation. The procedure was repeated for successively longer cracks which were grown by reinserting the wedge. When the fracture surfaces were examined under an optical microscope, the surfaces of the mode I cracks were much smoother than those of the mode II cracks. The greater smoothness of the crack faces generated under mode I loading led to compliance values (Figure II) that were larger than any of the other measured values. The lower compliances that were measured for mode II cracks were probably due to interlocking of the rough fracture surfaces that were produced by the 45° microcracking noted earlier. This supposition is further borne out by the fact that the compliance of the specimens containing fatigue mode II starter cracks was greater than that of the specimens having arrested mode II starter cracks. Presumably the fatigue-induced motion of the crack faces smoothed out aspe-

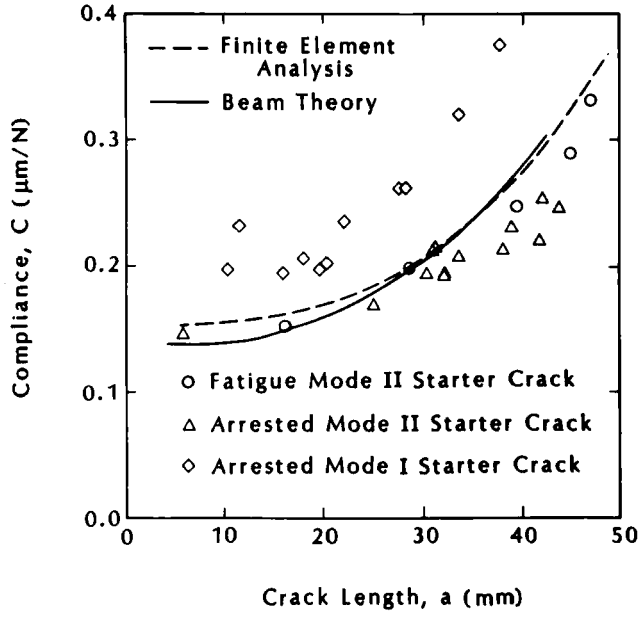

FIGURE 11 Comparison of measured and predicted ENF compliance.

rities. The differences in measured compliances may therefore be linked to differences in the frictional effects associated with the three types of fracture surfaces. However, the measured compliances are inconsistent with the predicted values which were obtained on the basis of crack faces that were coplanar with the adhesive midplane and which had further indicated that frictional effects were unimportant. The inconsistency arises because the measured compliances of the mode I cracks, which should have been in closest agreement with predictions, were considerably higher. In fact, the predictions were closest to the compliances of the fatigue mode II starter crack, especially for longer cracks. It is unclear at this time how the inconsistency can be resolved, but its effect on strain energy release rates (Figure 12) is strong because the compliance slopes are involved [Eq. (1)].

The strain energy release rates shown in Figure 12 were obtained from the compliances of Figure 11 and a reference load of 4.45 kN. For a given load level, it can be seen that the greatest amount of strain energy available for crack growth would be derived from the mode I starter cracks. The strain energy release rates derived from beam theory and finite element analyses are the next highest (except for very short cracks) and are reasonably consistent. The results for the mode II starter cracks are also consistent for crack lengths up to $a/L < 0.50$ in that they are approximately equal to or lower than the analytical values and more energy is available for fracture when the starter cracks were produced by fatigue instead of arrest. For longer cracks, the strain energy available for crack growth is lower for the fatigue starter cracks, which is inconsistent with the idea that asperities have

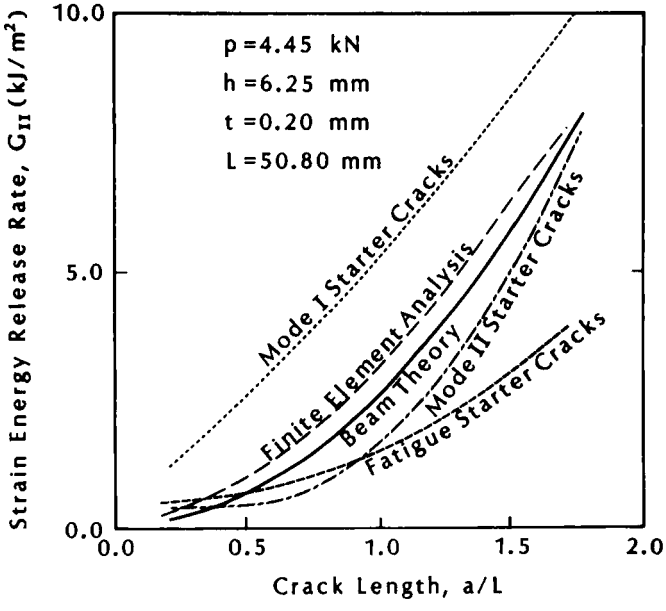

FIGURE 12 Mode II strain energy release rates derived from various compliances.

Downloaded At: 15:14 22 January 2011

been smoothed out and frictional effects are smaller. The inconsistency may be due to the fact that strain energy release rates derived from compliances are sensitive to the way in which the compliance slopes are obtained and emphasizes that the method should be used with care.

The finite element analyses with and without crack face contact all confirmed that an ENF specimen containing a smooth cohesive crack along the adhesive midplane produces pure mode II conditions. The fracture toughnesses derived from the measured compliances and equation (1) are shown in Figure 13. The data are identified by specimen number and, with the exception of specimen #4, specimens both with and without fatigue starter cracks exhibited increases in toughness with crack length. The large degree of scatter was also reflected in the toughness values obtained from beam theory and finite element analyses. The toughness derived from the measured compliance of arrested starter cracks was 1.59 kJ/m^2, with a coefficient of variation of 42%. Some of the scatter is probably due to difficulties in determining the location of the main crack tip and whether or not linking between microcracks had occurred. Higher toughnesses were calculated from the beam theory and finite element analysis (Table I) for the reasons noted in the discussion of Figure 12.

It was thought that the apparent increases in mode II toughnesses noted in Figure 13 might be due to crack tip fields interacting with those of the central load point. While such extensive interactions could not occur under linearly elastic conditions, the possibility of elastoplastic behavior giving rise to long plastic zones

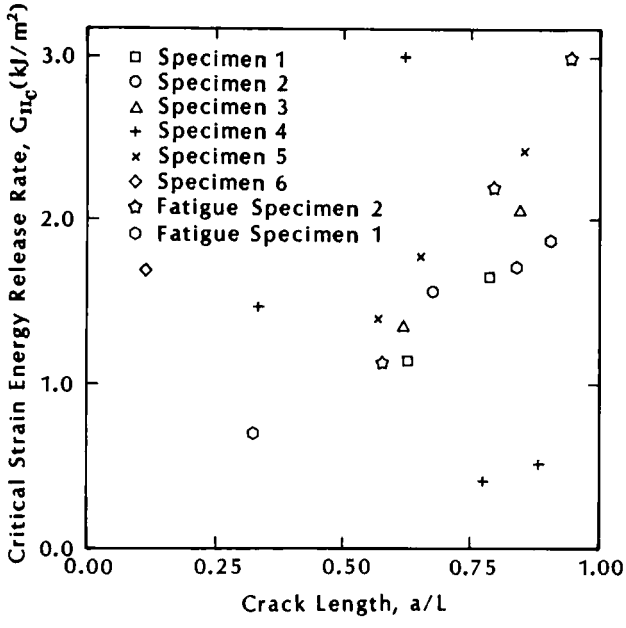

FIGURE 13 Mode II fracture toughness of FM300.

Downloaded At: 15:14 22 January 2011

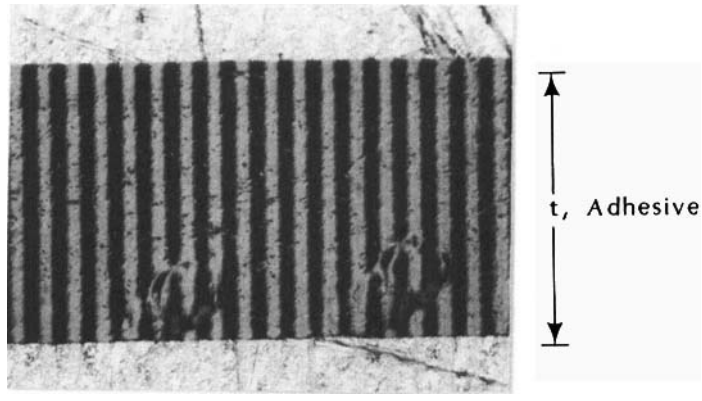

FIGURE 14 Initial Photoresist pattern deposited on the adhesive layer.

ahead of the crack was investigated. The constraint applied by the adherends has been shown in the past to elongate plastic zones[5,27,31] and was considered further in the present context with some preliminary Moiré grid measurements and elastoplastic analyses.[32]

In order to measure the deformations in the adhesive layer, a thin (1.5 μm) layer of photoresist was applied to the polished edges of an ENF specimen. The photoresist was exposed to a 40 line per mm grating and developed to produce the pattern shown in Figure 14. During a test, a region of interest was observed through a microscope to which a video camera, subtractor, recorder and monitor were attached. The initial grating was stored in one memory of the video subtractor and subtracted in real time from subsequent frames that were taken as the load increased. This procedure yields a series of Moiré fringes which are contours of constant displacement in the direction perpendicular to the initial grating. The displacement, u, along some fringe, N, is given by

$$u = Np \tag{6}$$

where p is the initial grating pitch (0.025 mm). The u-displacement contours ran parallel to the bondline, indicating shear; but one fringe essentially occupied the 0.2 mm adhesive layer thickness, making it difficult to determine the u-displacement distribution through the thickness of the adhesive. Higher frequency gratings would increase the resolution. Fortunately, it was possible to observe the shear deformations corresponding to critical loads without the Moiré effect, as can be seen from the sketch (Figure 15) of the permanent deformation ahead of a crack following a loading and unloading cycle. An interesting feature of the deformation is that it was localized in the scrim plane. In this instance, the grid was deformed for a distance $a/L = 0.175$ ahead of the crack tip, indicating that some of the longer cracks in Figure 13 were too close to the central load point to yield meaningful data.

The elastoplastic stress analysis of an ENF specimen with $a/L = 0.625$ and

Downloaded At: 15:14 22 January 2011

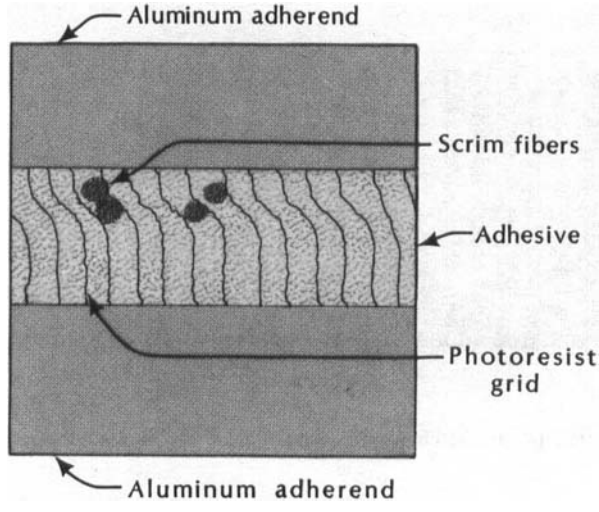

FIGURE 15 Deformed grid ahead of the crack tip

Downloaded At: 15:14 22 January 2011

$P = 3.2$ kN predicted that the Von Mises equivalent stress contours would have the form shown in Figure 16. Level 2 (22.75 MPa) corresponds to initial yielding, and so the plastic zone fully occupied the adhesive a distance 0.225 L ahead of the crack tip (outside the field of view of Figure 16). Such a large plastic zone seems reasonable in light of the grid observations, although more detailed measurements are required for a more rigorous comparison. Nonetheless, it is again clear that some of the starter cracks (say $a/L > 0.75$) in Figure 13 were too long for meaningful data to be extracted. If all arrested starter crack data for $a/L > 0.75$ and the results from specimen #4 (spurious) and #5 (too short a crack) are rejected, then an average G_{IIc} of 1.40 kJ/m^2, with a coefficient of variation of 16%, results. Although an elastoplastic analysis was not conducted for the MMF

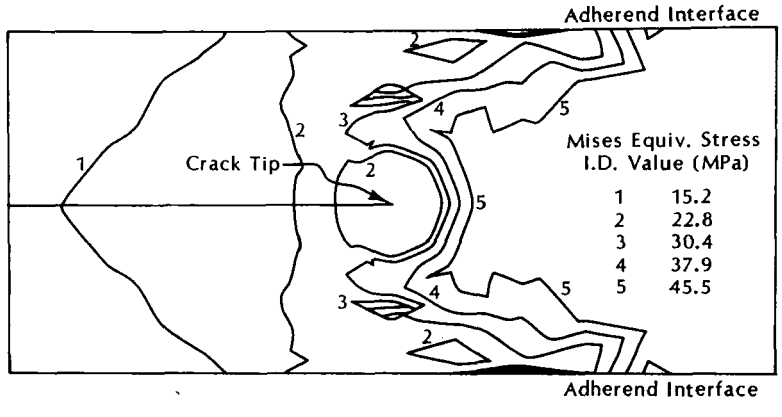

FIGURE 16 Von Mises equivalent stress contours around a cohesive crack in an ENF specimen.

specimen, the results of the ENF study indicate that mixed-mode toughness data should not be taken for $a/L > 0.75$.

Fracture envelope

The results of the tests with the DCB, MMF and ENF specimens are summarized in the fracture envelope shown in Figure 17. The toughness values that were used in the plot were the mean values noted in the discussion of the results from each specimen.

The values indicate that the mode I and mixed-mode toughnesses were much the same, but that the mode II toughness was 42% higher, albeit with greater scatter. The modified value of G_{II_C} was greater than G_{I_C} by 25%, which was just

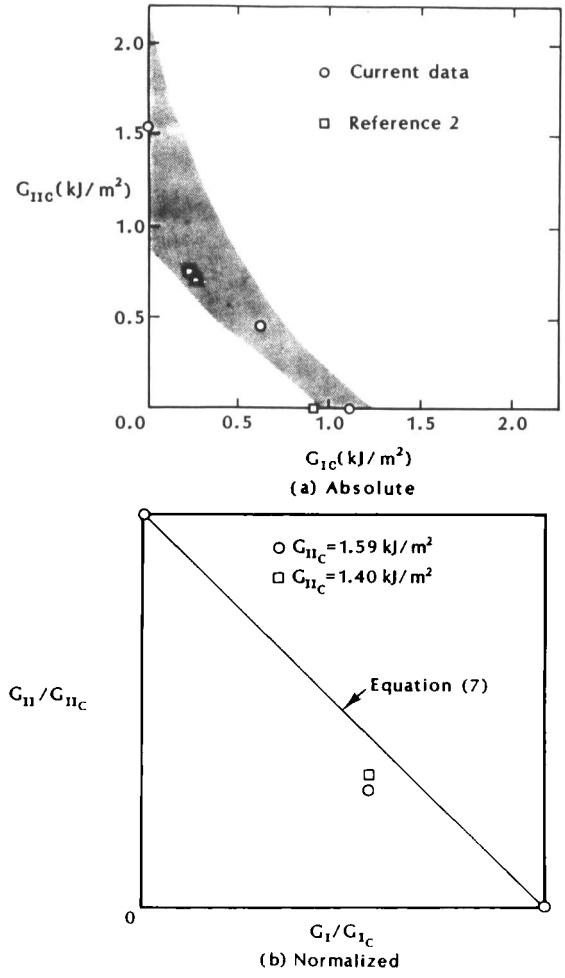

FIGURE 17 Fracture toughness envelope of FM300.

Downloaded At: 15:14 22 January 2011

within the combined coefficients of variation of any of the toughness values. The least that can be said is that, for FM300, the criterion

$$\frac{G_I}{G_{I_c}} + \frac{G_{II}}{G_{II_c}} = 1 \tag{7}$$

holds (Figure 17b) where $G_{I_c} \neq G_{II_c}$. However, it is quite possible (particularly from the lower bound to the data) that the simpler criterion

$$G_I + G_{II} = G_{I_c} = G_{II_c} = G_{T_c} \tag{8}$$

is valid if the scatter is reduced and the causes of increasing toughness are resolved. From the design point of view (8) is attractive for its simplicity.

It is important to note at this point that the average toughness values obtained by beam theory and finite element analysis (Table I) display an increasing toughness with increasing mode II component. Whereas the measured compliances gave rise to G_{I,II_c} values that were slightly lower than the G_{I_c} values, the mixed-mode toughness was notably higher than the mode I value obtained from beam theory and finite element calculations. Furthermore, the mode II toughnesses obtained from the latter two methods were higher than the corresponding values from compliance calculations. The result is that the fracture envelope (Figure 18) follows the criterion of Eq. (7) more closely, although it is clear from the compliance comparisons (Figs. 7, 9, 11) that shifts in toughness can be expected when different methods are used for their calculation. However, the results summarized in Table I and Figure 18 indicate that the shifting may not be in the same direction for all mode-mixes, which then affects the shape of the fracture envelope and influences the choice of mixed-mode fracture parameter. The toughness values based on compliance measurements were used in Figure 17 because they are direct and can be used by a wider population. The Achilles heel of the method is obtaining the derivative $\partial C/\partial a$.

Since FM300 is considered to be a tough adhesive, the results of Figure 17 are in agreement with those of Refs 2, 12, 13, 14, 26. The decrease in toughness for intermediate mode-mixes that was noted in the review[5] of work using the scarf and ILMMS specimens was very mild here. The main reason for the lack of such a decrease in the present study may have been that the microcracks did not extend to the boundary between the adherends and adhesive before linking. The results of the present study do not agree with a recent study[29] where the effect of bond thickness on G_{II_c} and G_{III_c} was considered. G_{II_c} and G_{III_c} were essentially the same, but were up to 40 and 15 times higher than G_{I_c} for a brittle and tough adhesive, respectively, at common bond thicknesses. Equality in all three toughnesses could only be seen when the results were extrapolated to submicron bond thicknesses. The adhesives used in Ref. 29 were neither scrimmed nor did they contain glass beads[12,13,14,26] for maintenance of bondline thickness. For equivalent thicknesses, the G_{II_c} values obtained for a tough adhesive in Ref. 29 were 10–15 times higher than those obtained here and in Refs. 12, 13, 14, 26. The

Downloaded At: 15:14 22 January 2011

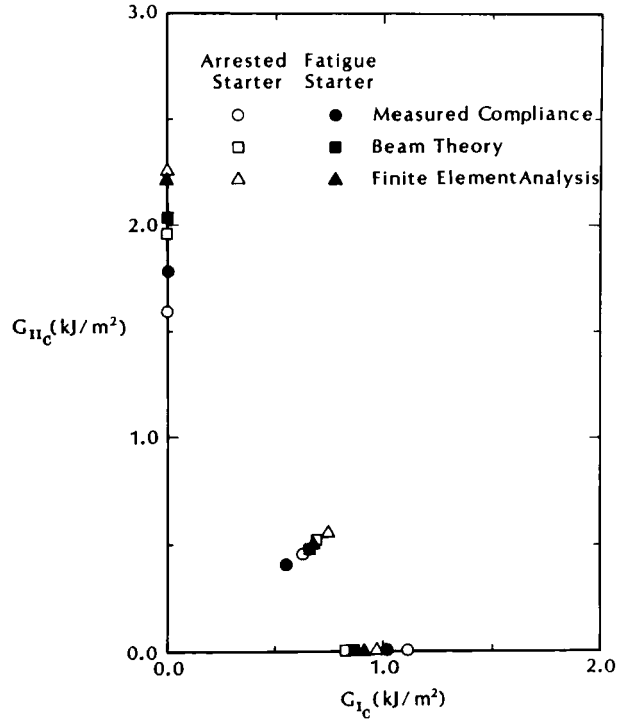

FIGURE 18 Comparison of fracture envelopes depending on method of data reduction

Downloaded At: 15:14 22 January 2011

association is right at hand that such inclusions decrease the mode II toughness by promoting the mode I microcracking, and therefore overall fracture, at lower loads, thus decreasing the overall toughness of the material.

A further complication has been noted in another recent study[33] where FM300K was tested in mode I and mode I–III. The FM300K designation indicates that the scrim is an open knit cloth carrier instead of the tricot knit carrier (FM300) used in this study and those in Refs. 11 and 12. It was found[33] that the mixed-mode toughness of FM300K was twice its mode I value. The reason for the difference was that under mode I cracking the open knit carrier separated from the adhesive without being torn itself, whereas the nature of crack growth in mode I–III gave rise to tearing of the cloth which in turn gave rise to more energy dissipation and higher overall toughness. Thus, although the open knit scrim acts as a stress concentrator in the same way that the tricot knit does, the open knit may have to be torn under certain conditions in order for propagation of the main crack to occur. However, the special conditions may only exist in cases where cracking in the joint initiates on opposite sides of the carrier from different edges. Thus, the tearing of open knit carrier might not occur in the types of tests considered here where there is only one crack.

CONCLUSIONS

Simple laminated beam geometries cut from the same laminated plate but loaded in slightly different ways have been used to define the full mixed-mode fracture envelope for a structural adhesive. The specimen sizes were relatively small so that small amounts of adhesive would be required for evaluating new formulations and surface preparations in a direct manner. The testing and data reduction methods were developed for aluminum adherends bonded with FM300, a relatively tough adhesive. Mode I and mixed-mode ($G_I/G_T = 57\%$) fracture toughnesses were determined from double cantilever beam (DCB) and mixed-mode flexure (MMF) specimens and were the same with reasonable degrees of scatter. The mode II fracture toughness was obtained from end-notched flexure (ENF) specimens. When all the data were included, G_{II_c} was 60% higher than G_{I_c}. However, there was a notable increase in toughness values with crack length when either arrested or fatigue starter cracks were used. When the higher values from each specimen were neglected along with some other spurious results, the new average G_{II_c} was essentially the same as G_{I_c}, making the total energy release rate an appropriate mixed-mode fracture parameter. An elastoplastic finite element stress analysis and some preliminary grid measurements indicated that some of the increase in toughness could be accounted for by interactions between central load point fields and rather long zones of permanent deformation that were at least 20% of the specimen semi span ($5.0t$). Accordingly, it is recommended that ENF and MMF tests for tough adhesives be conducted for $0.25 < a/L < 0.75$.

Overall crack growth was preceded by whitening around scrim fibers and tensile microcracking ahead of the main crack tip. The orientation of the microcracks varied with specimen type, running from 0° for the DCB through 25°–30° for the MMF and 45° for the ENF specimens, in correspondence with the maximum principal stress directions in the adhesive layer of each of the specimens. Thus, as had been noted in earlier work[3,5,29] the adhesive itself always fails by mode I microcracking and subsequent linking, although the analysis of the specimens used here indicated that cohesive cracks coplanar with the adhesive mid plane provide 57% and 0% G_I/G_T in the MMF and ENF specimens. The challenge for future work is to be able to predict the onset of microcracking and the interactions of the microcracks with the main crack under various mode-mixes.

Downloaded At: 15:14 22 January 2011

Acknowledgements

This work was supported under the DARPA/ONR High Temperature Adhesives Program through a subcontract from Hughes Aircraft Company; the support is gratefully acknowledged. Many thanks are also due to Jeanie Paterson who prepared the manuscript.

References

1. W. S. Johnson and P. D. Mangalgiri, in *Toughened Composites, ASTM STP 937*, N. J. Johnston, Ed. (American Society for Testing and Materials, Philadelphia 1987), pp. 295–315.

2. E. J. Ripling, S. Mostovoy and H. T. Corten, *J. Adhesion* **3,** 107(1971).
3. G. C. Trantina, *Journal of Composite Materials* **6,** 371 (1972).
4. W. D. Bascom, R. L. Cottington and C. O. Timmons, *J. Appl. Polym. Science* **32,** 165 (1977).
5. E. Sancaktar, H. Jozavi, J. Baldwin, J. Tang, *J. Adhesion* **23,** 233 (1987).
6. Y. W. Mai and A. S. Vipond, *J. Materials Science* **13,** 2280 (1978).
7. T. R. Brussat and S. T. Chiu, *J. Engineering and Technology* **100,** 39 (1978).
8. R. A. Everett, Jr. and W. S. Johnson, in *Delamination and Debonding of Materials, ASTM STP 876,* W. S. Johnson, Ed. (American Society for Testing and Materials, Philadelphia, 1985), pp. 256–281.
9. C. Lin and K. M. Liechti, *J. Adhesion* **21,** 1 (1987).
10. S. Mall, W. S. Johnson and R. A. Everett, Jr., in *Adhesive Joints: Their Formation, Characteristics and Testing,* K. L. Mittal, Ed. (Plenum Press, New York 1984), pp. 639–658.
11. W. S. Johnson and S. Mall, in *Delamination and Debonding of Materials, ASTM STP 876,* W. S. Johnson, Ed., (American Society for Testing and Materials, Philadelphia, 1985), pp. 189–199.
12. S. Mall and W. S. Johnson, in *Composite Materials: Testing and Design (Seventh Conference), ASTM STP 893,* J. M. Whitney, Ed. (American Society for Testing and Materials, Philadelphia, 1986), pp. 322–334.
13. S. Mall, M. A. Rezaizadeh and R. Gurumurthy, *J. Engineering Materials and Technology* **109,** 17 (1987).
14. S. Mall and K. T. Yun, *J. Adhesion* **23,** 215 (1987).
15. W. S. Johnson, *J. Testing and Evaluation* **15,** 303 (1987).
16. B. Dattaguru, R. A. Everett, Jr., J. Whitcomb, and W. S. Johnson, *J. Engineering Materials and Technology* **106,** 59 (1984).
17. P. S. Vanderkley, "Mode I – Mode II Delamination Toughness of a Unidirectional Graphite/Epoxy Composite," M.S. Thesis, 1981, Texas A&M University, Mechanics and Materials Center Report # MM 3724-81-15.
18. J. G. Williams, *Intern. J. of Fracture* **36,** 101 (1988).
19. A. J. Russell and K. N. Street, in *Progress in Science and Engineering of Composites,* T. Hayashi, K. Kawata, and S. Unekawa, Eds., (ICCM-IV, 1982), pp. 279–286.
20. A. J. Russell and K. N. Street, in *Delamination and Debonding of Materials, ASTM STP 876,* W. S. Johnson, Ed. (American Society for Testing and Materials, Philadelphia, 1985), pp. 349–370.
21. A. J. Russell and K. N. Street, in *Toughened Composites, ASTM STP 937,* N. J. Johnston, Ed. (American Society for Testing & Materials, Philadelphia, 1987), pp. 275–294.
22. G. S. Giore, *Engineering Fracture Mechanics* **20,** 11 (1984).
23. L. A. Carlsson, J. W. Gillespie, and R. B. Pipes, *J. Composite Materials* **20,** 594 (1986).
24. G. B. Murri and T. K. O'Brien, AIAA Paper 85-0647, Proceedings of the 26th AIAA/ASME/ASCE/AHS Structures, Structural Dynamics and Materials Conference, Orlando, FL, 1985.
25. S. Mall and N. K. Kochar, *J. Composite Technology and Research* **8,** 54 (1986).
26. S. Mall and N. K. Kochar, *Proceedings of the Institution of Mechanical Engineers, IMechE* **6,** 71 (1986), Paper # C159/86.
27. P. D. Mangalgiri, W. S. Johnson, and R. A. Everett, Jr., *J. Adhesion* **23,** 263 (1987).
28. H. Chai and S. Mall, *Intern. J. of Fracture* **36,** R3 (1988).
29. H. Chai, *ibid.* **37,** 137 (1988).
30. T. Freda, "The Use of Laminated Beams for the Determination of the Pure and Mixed-Mode Fracture Properties of Adhesives," Master's Thesis, The University of Texas at Austin, Engineering Mechanics Research Laboratory, Report Number EMRL 87/5, (1987).
31. S. S. Wang, J. F. Mandell, and F. J. McGarry, *Intern. J. of Fracture* **14,** 39 (1978).
32. E. H. Catsiff, T. K. Dougherty, W. E. Elias, D. J. Vachon, R. W. Seibold, W. G. Knauss, S. Shimabukuro, and K. M. Liechti, "High Temperature Adhesive Systems," Interim Report for the period September 1985–January 1988. Hughes Aircraft Company, El Segundo, CA (1988).
33. E. J. Ripling, P. B. Crosley and W. S. Johnson, in *Adhesively Bonded Joints: Testing, Analysis and Design, ASTM STP 981,* W. S. Johnson, Ed. (American Society for Testing and Materials, Philadelphia, 1988), pp. 163–182.

Downloaded At: 15:14 22 January 2011